Journal of Fluids and Structures (1999) **13,** 579–606
Article No.: jfls. 1999.0220, available online at http://www.idealibrary.com on IDEAL

THE FLOW INTERACTION BETWEEN A STATIONARY CYLINDER AND A DOWNSTREAM FLEXIBLE CYLINDER

D. Brika and A. Laneville

Département de Génie mécanique, Université de Sherbrooke
Sherbrooke, Québec, Canada J1K 2R1

(Received 10 August 1998 and in revised form 15 March 1999)

This paper deals with an experimental investigation of the dynamic response of a long flexible circular cylinder in the wake of a stationary geometrically similar cylinder. The system has a low damping ratio. The tandem and staggered arrangements have been considered. The separations investigated are typical of transmission line bundles and range from 7 to 25 diameters and Reynolds number ranges from 5 000 to 27 000. For the tandem cylinders, the results indicate that (a) the dynamic response of the downstream cylinder is no longer hysteretic, (b) the synchronization onset is at higher reduced velocities and (c) the synchronization region is wider than that of an isolated cylinder; this region is twice as large for a separation of 10 diameters and decreases with increasing spacing. Despite the absence of the hysteresis loop and its associated discontinuities, two vortex patterns are present around the resonance velocity. A small decrease of the maximum amplitude of oscillation with increasing spacing has also been observed, as well as a reduction of the velocity for which this maximum occurs. For separations of 7 and 8·5 diameters, the leeward cylinder exhibits a combination of vortex-induced and wake-galloping oscillations. For the staggered arrangement, the increase of the stagger angle β reduces the synchronization onset velocity and the synchronization region and beyond $\beta = 20^\circ$, the downstream cylinder behaves as an isolated one.

1. INTRODUCTION

The vortex-induced vibration of a circular cylinder has attracted many researchers for quite a long time. The different studies, as summarized by Sarpkaya (1979), Bearman (1984), Parkinson (1989) and Blevins (1990), show the complexity of this phenomenon. When a cylinder is immersed in the wake of another cylinder, the flow pattern gains in complexity as shown in the reviews of Zdravkovich (1977, 1988) and Chen (1986). The wake interference between cylinders has many engineering applications, such as transmission lines, suspension bridges and heat exchangers, the integrity of which is a major concern.

It is foreseeable that a cylinder located in the wake of another will not behave as would an isolated one. The fluctuating components, the vortices shed from the upstream cylinder and the reduced mean velocity of the wake flow impinging on the downstream cylinder, are parts of the rationale leading to this prediction. In the relatively simple case of two stationary cylinders, the experimental results support this point of view [see Ohya *et al.* (1989)]; the aerodynamic parameters such as the drag and lift forces, the pressure distribution, the Strouhal number and the vortex-shedding patterns differ significantly and depend strongly on the spacing L between the centres of the cylinders. The most important result in this case is the presence of a discontinuity in these characteristics at a critical spacing ratio L/D ranging between 3·5 and 4; D is the cylinder diameter.

0889–9746/99/050579 + 28 $30.00

In the case of one cylinder vibrating in the wake of another fixed one, the interaction between the wake flow and the oscillating cylinder becomes complex, as has been reported in the experiments of Tanida *et al.* (1973), Price (1975), King & Johns (1976) and Bokaian & Geoola (1984) among others. The discontinuity observed in the region $3{\cdot}5 < L/D < 4$ with stationary models, was not noted in the experiments of Tanida *et al.* (1973) and King & Johns (1976) in which both cylinders were free to vibrate. For $2{\cdot}5 < L/D < 7$, the downstream cylinder continued to vibrate with fairly uniform amplitude well beyond the synchronization region of the upstream cylinder. This phenomenon has received different definitions: "interference galloping" (Ruscheweyh 1983), "galloping" (Bokaian & Geoola 1984) and "wake-displacement excitation" (Zdravkovich 1988). Bokaian and Geoola observed that, depending on the separation and structural damping of the cylinders, the downstream cylinder may exhibit vortex-resonance, galloping, combined vortex-resonance and galloping, or separated vortex-resonance and galloping. The vortex-resonance was observed for relatively higher separations ($L/D > 3$), while the other phenomena were observed when the two cylinders are closer to each other.

Cooper & Wardlaw (1971) observed "wake galloping" where the cylinder undergoes catastrophic amplitudes which may reach 20 diameters. The path of motion in this case is elliptical with the minor axis fairly perpendicular to the wind direction. Wake galloping occurs for separations similar to those encountered in transmission line bundles ($10 < L/D < 20$) and when the downstream cylinder is slightly displaced from the wake centre-line of the upstream cylinder, i.e., for a bundle angle β with respect to the flow direction between 10° and 30°.

In addition to L/D, the plane of vibration influences the dynamic response of the cylinder (Brika & Laneville 1995a) as well as the vortex patterns in its near-wake (Öngören & Rockwell 1988). The stiffness of the separating rods in conductor bundles may lead to vibrations in planes other than the orthogonal and in-line ones.

The aim of the present study is, then, to investigate experimentally the influence of L/D and the plane of vibration on the dynamic response of a long flexible circular cylinder immersed in the wake of a similar stationary cylinder when damping is low. Tandem and staggered arrangements are examined. The study also addresses the following question: how will the presence of a fixed upstream cylinder affect the hysteresis, discontinuities and bifurcation phenomena and the two modes of vortex shedding controlling these phenomena as observed in the case of an isolated cylinder (Brika and Laneville 1993, 1995a)? The results will be discussed in the light of those pertaining to a single cylinder.

2. EXPERIMENTAL SET-UP

Figure 1 shows a schematic diagram of a bundle of two cylinders and the different parameters studied, i.e., the separation L between the cylinders, the plane of vibration angle, α, and the inclination β of the bundle. The upstream cylinder is fixed, while the leeward one is freely excited by wind in different planes, α, with respect to the cross-flow direction. The experimental set-up of the downstream cylinder and the instrumentation used are described in more detail in Brika & Laneville (1993). It essentially consists of a long tube suspended horizontally in the wind tunnel test-section with thin steel flexible blades at the nodes of its first free–free vibration mode. The nodes coincide with the tunnel walls and the part of the model internal to the wind tunnel vibrates in a quasi-sinusoidal mode shape. The model supporting system can be oriented in different directions, allowing vibrations in different incident planes. Both cylinders have smooth surfaces and the same external diameter $D = 33{\cdot}4$ mm. The natural frequency of the oscillating model is $f_n = 17{\cdot}58$ Hz, and the vibrating system has a low damping ratio $\zeta = 0{\cdot}83 \times 10^{-4}$ (where $\zeta = c/2M\omega_n$, c being the

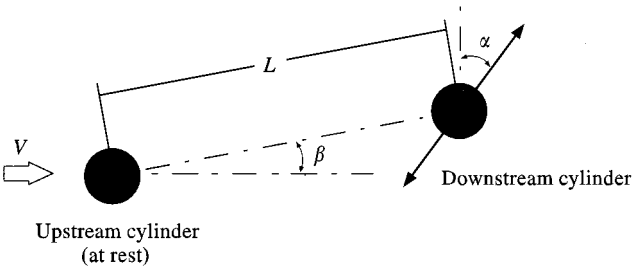

Figure 1. Schematic view of a bundle of two cylinders.

TABLE 1.
Experimental test matrix

Constant	Variable	$\alpha = 0°$	15°	30°	45°
$\beta = 0°$	L/D	7	*	*	*
		8·5	*	*	*
		10	10	10	10
		13	13	13	13
		16	16	16	16
		25	25	25	25
$L/D = 13$	β	5°	5°	5°	5°
		10°	10°	10°	10°
		15°	15°	15°	15°
		20°	20°	20°	20°

damping coefficient, M the mass of the vibrating system, and ω_n the circular natural frequency). The blockage ratio of the models in the test-section is about 1·8%, and the aspect ratio, $l_e/D = 52{\cdot}7$, where l_e is the net length of the cylinder exposed to the air-flow.

The cylinder displacement is measured with a B&K 4393 accelerometer and the vortex shedding frequency with a hot-wire anemometer located at the model mid-span, 1·5D downstream and 1·5D below the downstream cylinder axis in its stationary position. The signals of both instruments are examined on a B&K 2032 frequency analyser. The phase difference, Φ, between the hot-wire output and the cylinder displacement as well as the accelerometer signal are also recorded on a dual channel Brush recorder. The measured phase must be regarded as a relative characteristic, since the anemometer is stationary and at a distance from the cylinder in motion.

Six separations, L/D, have been tested with the cylinders in tandem, namely $L/D = 7$, 8·5, 10, 13, 16 and 25, as well as five values for the bundle inclination angle β, namely $\beta = 0$, 5, 10, 15 and 20° for a separation $L/D = 13$, typical of transmission line bundles. For each value of these two parameters (except $L/D = 7$ and 8·5), the planes of vibration were $\alpha = 0$, 15, 30 and 45°. The experimental test matrix (Table 1) summarizes the combination of the different parameters examined. The Reynolds number, Re, ranges between 5 100 and 27 500.

3. ISOLATED CYLINDER

To establish a baseline, the results obtained with a single cylinder using the same experimental setup are presented. These will serve as a reference in the analysis of the effect of a fixed cylinder on the dynamic response of the downstream cylinder. The results of an isolated cylinder are presented in more detail by Brika & Laneville (1993, 1995a). Figure 2 summarizes the data of Brika & Laneville (1993) and shows the relative amplitude A/D, the vortex-shedding frequency and the phase angle Φ as a function of the reduced velocity $V_r = V_\infty/fD$, where A being the single amplitude at mid-span and V_∞ the undisturbed flow velocity. The vibration frequency f as expected in lock-in cases remains practically constant and equal to the model natural frequency ($f \approx f_n = 17{\cdot}58$ Hz). Briefly, the results indicate that synchronization is sustained between $V_r = 4{\cdot}9$ and $7{\cdot}5$, and that the cylinder response is hysteretic. The hysteresis is characterized by two branches and two discontinuities and, as observed by flow visualization (Brika & Laneville 1993), each branch is associated with a particular vortex pattern in the cylinder wake. The upper branch, ranging between the synchronization onset and $V_r = 6{\cdot}3$ and generally obtained with a progressive increase of flow velocity, is associated with a vortex pattern referred to as the *2S mode* (Williamson & Roshko 1988), where a single vortex is shed from each side of the cylinder at every cycle of vibration. The lower branch, ranging between the end of synchronization and $V_r = 5{\cdot}5$, is obtained either with a progressive reduction of the flow velocity or with a release of the cylinder from rest, or from a high amplitude, and is associated with the *2P mode*, where a pair of vortices of opposite signs is shed from each side of the cylinder at every cycle of vibration. The jumps are attributed to sudden changes from one mode to the other.

4. TANDEM ARRANGEMENT

4.1. General Tendency of the Dynamic Response

Figure 3 shows the effect of the separation ratio L/D on the dynamic response of the downstream cylinder for different planes of vibration when the two cylinders are in a tandem arrangement. Compared to the results obtained with an isolated cylinder (solid lines with no symbols), it appears clearly that the dynamic response of the leeward cylinder is considerably modified by the presence of a fixed upstream cylinder. The hysteresis phenomenon has completely disappeared as well as the sudden jumps in the vibration amplitude. The dynamic response is indeed described by a single and continuous curve. Figure 3 also indicates that, for each plane of vibration, the synchronization onset for the leeward cylinder is at a higher velocity, while it occurs around $V_r = 4{\cdot}9$ in the case of an isolated cylinder. This difference is attributed to a lower flow velocity in the wake of the upstream cylinder. The synchronization onset velocity varies slightly with L/D and this variation appears clearly at $\alpha \geq 30^\circ$. The figure also shows that the synchronization region of the downstream cylinder is larger than that of an isolated one. In the case $\alpha = 0^\circ$, this synchronization region is twice as large for a separation $L/D = 10$, and it decreases with increasing value of L/D. The maximum vibration amplitude of the downstream cylinder for $L/D = 10$ is of the same order as that obtained with an isolated cylinder. This maximum amplitude, as well as the resonance velocity, V_{res}, decreases slowly with increasing value of the spacing ratio L/D. Up to the largest spacing ratio tested ($L/D = 25$), the leeward cylinder response remains different from that of an isolated cylinder and the upstream cylinder can still be said to influence the response of the downstream one.

The results shown in Figure 3 also present a first, but smaller, peak at $V_r \approx 5$ where the response seems to coincide with that of an isolated cylinder. In fact, at $V_r = 5$, the vortices shed from the upstream cylinder have a frequency approximately equal to the natural

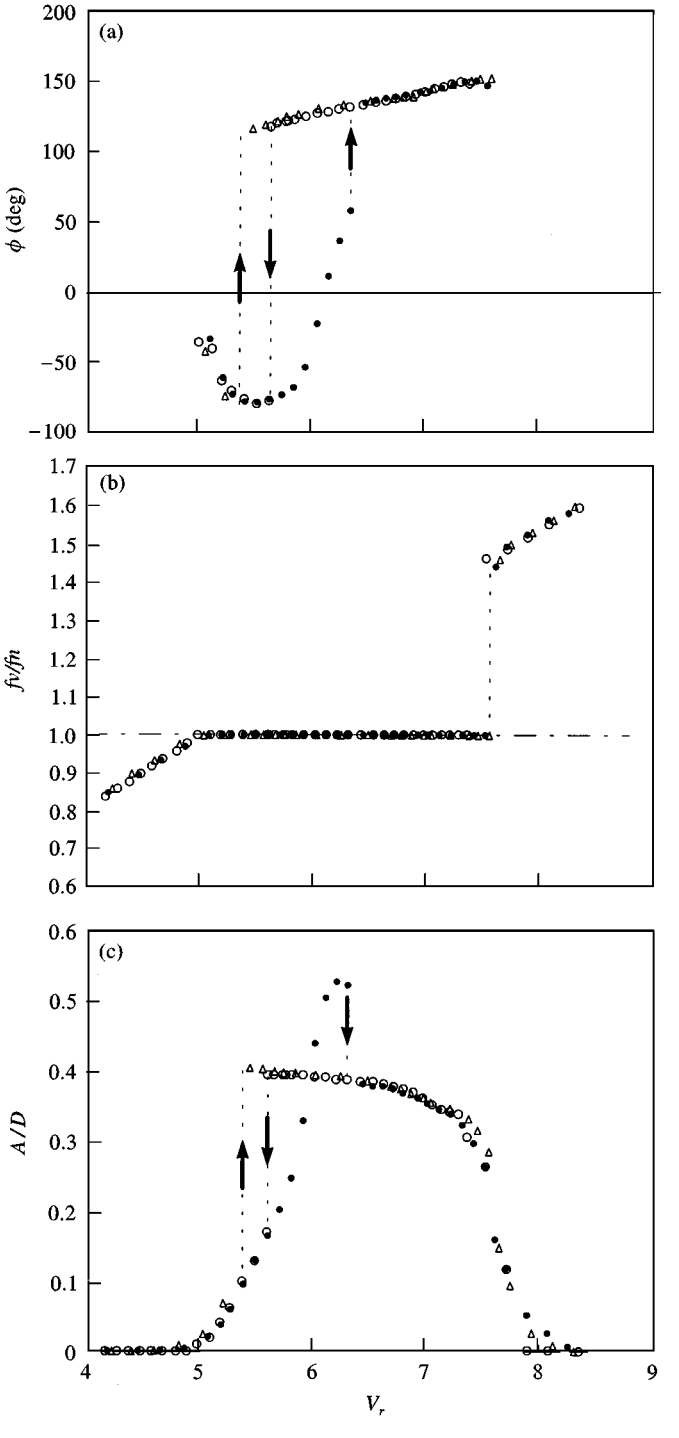

Figure 2. Characteristics of the response of an isolated cylinder as a function of the reduced velocity ($\alpha = 0°$): (a), phase angle Φ; (b) vortex-shedding frequency f_v; (c) amplitude of vibration. ●, Increasing velocity; △, increasing velocity with large steps; ○, decreasing velocity.

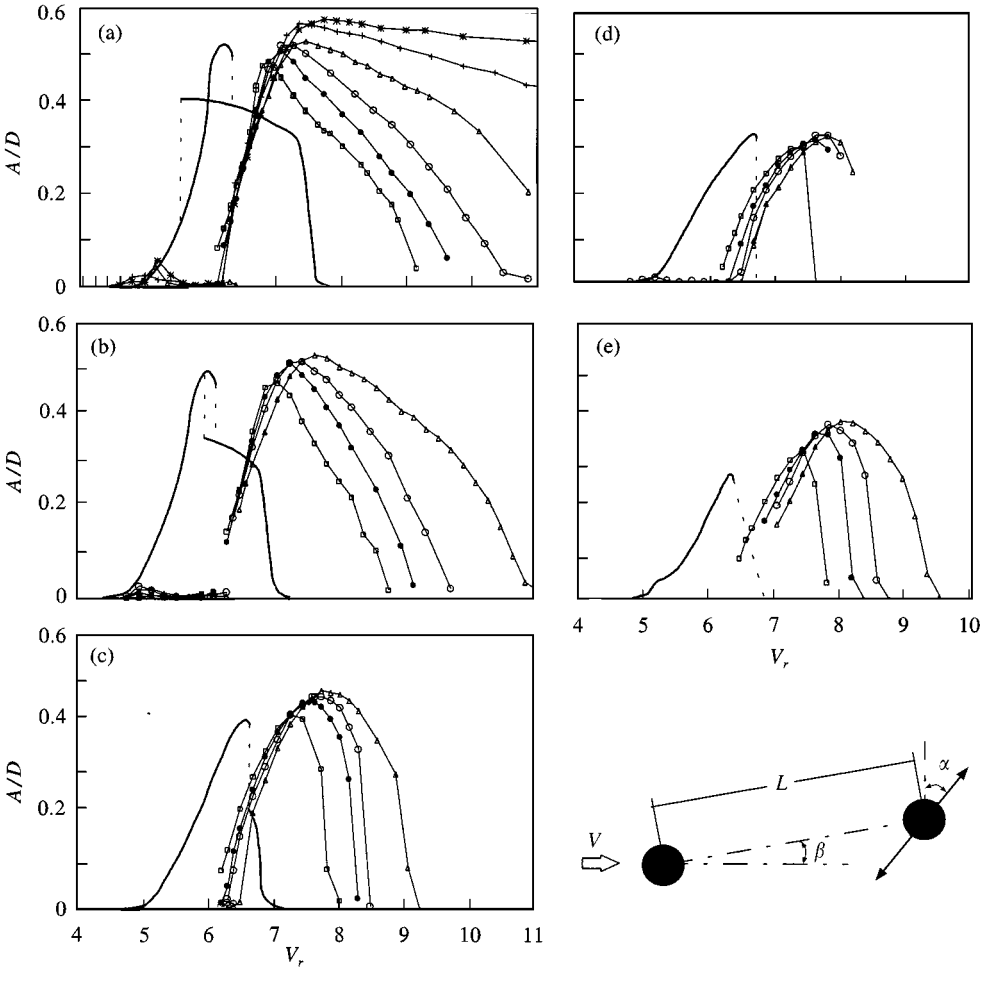

Figure 3. Effect of the spacing ratio L/D on the response of the downstream cylinder for the tandem arrangement: (a) $\alpha = 0°$; (b) $\alpha = 15°$; (c) $\alpha = 30°$; (d) $\alpha = 45°$; (e), $\alpha \sim -45°$. *, $L/D = 7$; +, 8·5; △, 10; ○, 13; ●, 16; □, 25; ––, single cylinder.

frequency ($f_n = 17{\cdot}58$ Hz) of the downstream cylinder: as they impinge on the leeward cylinder, these *synchronized* vortices trigger its oscillations. If the flow velocity is increased, the vortex-shedding frequency of the fixed cylinder departs from the value of $f_n = 17{\cdot}58$ Hz and this resonance ceases. When the model is released from rest, it is always stabilized on the steady-state amplitude curve obtained with a progressive variation of the flow velocity.

4.2. Special Case of $\alpha = 45°$

When the model supporting system is oriented in the direction $\alpha = 45°$, an intermediary position between the in-line and the cross-flow directions, vibrations in two different incident planes have been observed: the first, restrained by the direction of the blades ($\alpha = 45°$), and the other, perpendicular to it ($\alpha = -45°$). The same behaviour has also been observed with a single cylinder (Brika & Laneville 1995a). The results of the two planes are illustrated in Figure 3(d, e) with those of an isolated cylinder.

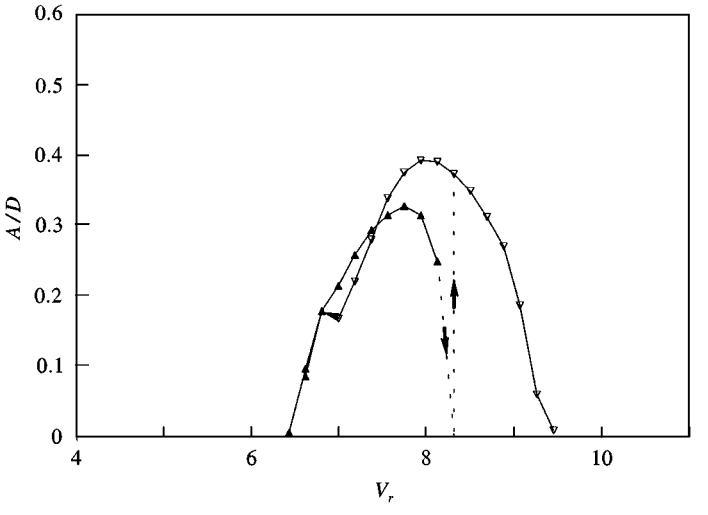

Figure 4. Comparison between the amplitudes of vibration in both planes $\alpha = \pm 45^\circ$ ($L/D = 10$, $\beta = 0^\circ$): ▲, $\alpha = +45^\circ$; ▽, $\alpha = -45^\circ$.

Figure 4 shows a comparison between the vibration amplitudes of the two orthogonal planes. The dotted lines with arrows indicate the direction of the switch from one plane of vibration to the other. The vibration in the chosen plane is dictated by the history of the motion, the flow velocity and the initial conditions of excitation. Indeed, if the reduced velocity is progressively increased from a lower value ($V_r < 6{\cdot}1$), the model vibrates in the direction $\alpha = +45^\circ$ and remains in this direction until the velocity $V_r = 8{\cdot}1$ is reached. Beyond this value, the amplitude vanishes and a vibration in the other plane ($\alpha = -45^\circ$) takes over. The oscillation remains in this plane for a further increase of the reduced velocity. If V_r is reduced from higher values, the cylinder also vibrates in the direction $\alpha = -45^\circ$ before reversing to the direction $\alpha = 45^\circ$ at $V_r = 6{\cdot}8$. The results shown in Figure 4 also reveal that, in general, the model vibrates with a slightly higher amplitude in the direction $\alpha = -45^\circ$ than in the direction $\alpha = 45^\circ$. The maximum amplitude of oscillation for the plane $\alpha = -45^\circ$ is, in fact, 20% greater than the one of $\alpha = 45^\circ$. The velocity at resonance for $\alpha = -45^\circ$ also appears to be greater than for the direction $\alpha = 45^\circ$.

When the downstream cylinder is released from rest, it oscillates in the direction $\alpha = -45^\circ$ over a wide range of the synchronization region, vibrating in the direction $\alpha = 45^\circ$ only over a narrow range of flow velocity near the beginning of synchronization. For the remaining portion of the range, it can vibrate in the $\alpha = 45^\circ$ direction only if it is initially pumped up with a shaker in the same direction with an amplitude greater than a limit value; otherwise, it turns back to the direction $\alpha = -45^\circ$. The limit amplitude of oscillation increases with increasing value of the reduced velocity as observed by Brika & Laneville (1995a).

4.3. Case of Small Separations

For the smallest separations examined, i.e., $L/D = 7$ and $8{\cdot}5$, another phenomenon has been observed. As illustrated in Figure 5(a), for $L/D = 8{\cdot}5$, the amplitude reaches a maximum at resonance and then decreases with increasing velocity. This tendency ceases to be similar to that in the cases where $L/D \geq 10$ since the cylinder does not stop vibrating as V_r becomes large; the vibration amplitude first reaches a minimum ($V_r = 16{\cdot}5$, $A/D = 0{\cdot}32$) and then

increases progressively with increasing V_r. The same scenario repeats itself for $L/D = 7$, the minimum occurring at ($V_r = 12{\cdot}2$, $A/D = 0{\cdot}53$) and the cylinder continues to vibrate with a maximum amplitude $A/D = 0{\cdot}58$ well beyond the resonance. A similar behaviour has been observed by Bokaian & Geoola (1984) at $L/D \leq 3$, King & Johns (1976) and Ruscheweyh (1983) at low Scruton number $\mathrm{Sc} = 2\,m(2\pi\zeta)/\rho D^2$ (m is the cylinder mass per unit length and ρ the fluid density). This behaviour is presumably a combination of two phenomena: vortex-induced vibrations and interference galloping. Interference galloping can be inferred to take over from the minimum. A comparison with the results of these authors will be examined in Section 4.5.

Figure 5(c) presents the vortex-shedding frequencies f_{v1} and f_{v2}, respectively, for the upstream cylinder (open circles) and the downstream cylinder (full circles) as obtained with the hot wire anemometer for the spacing ratio $L/D = 8{\cdot}5$. The frequency f_{v1} varies linearly with the reduced velocity according to the Strouhal relationship $f_{v1} = SV_\infty/D$, where S is the Strouhal number. For the present experimental results S corresponds to a value of 0·187. The vortex-shedding frequency, f_{v2}, of the downstream cylinder also varies linearly with the reduced velocity of the undisturbed flow, but with a reduced slope. The reduction of the slope of f_{v2} as a function of V_r can be attributed to a reduction of the mean flow velocity in the wake of the upstream cylinder. By relating the slopes of f_{v1} and f_{v2}, the mean flow velocity in the wake of the fixed upstream cylinder is estimated to be about 76% of the undisturbed flow velocity, V_∞, at a downstream distance of $8{\cdot}5D$. This value agrees with those of other studies [see Norberg (1998)]. Accordingly, the downstream cylinder begins to oscillate around $V_r \approx 6.4$, rather than around $V_r = 4{\cdot}90$ as in the case of an isolated cylinder. As f_{v2} approaches the natural frequency of the downstream cylinder ($f_n = 17{\cdot}58$ Hz), a resonant response of this cylinder tends to develop freely and f_{v2} locks-in to the cylinder frequency. For this particular separation ($L/D = 8{\cdot}5$) the lock-in phenomenon extends over a large range of flow velocity. In the case of larger separations, the frequency f_{v1} of the upstream cylinder does not appear in the spectra of the signal of the hot-wire anemometer.

The variation of the phase angle, Φ, between the vortex shedding and the cylinder displacement is presented as a function of the reduced velocity in Figure 5(b) for the spacing ratio $L/D = 8{\cdot}5$. The phase angle Φ increases rapidly with V_r between the synchronization onset velocity of the downstream cylinder and the velocity for which the maximum amplitude occurs (resonance velocity, V_{res}). In this range of reduced velocity, the phase undergoes a continuous and progressive variation on an interval of about 180°. Beyond the resonance velocity, Φ varies in a different manner; it increases slightly and linearly with V_r. The variation of Φ as a function of V_r is similar to that of an isolated cylinder, as shown in Figure 2; but, in this case, it is accompanied with a discontinuity. In this last figure, the branch of the phase angle curve ranging between the synchronization onset and resonance increases rapidly with V_r and is associated with the 2S mode of vortex shedding, while the other branch, which varies slightly with V_r, is associated with the 2P mode as have indicated the visualization results of Brika & Laneville (1993). From this analysis, two different patterns of vortex shedding seem to be present in the wake of the downstream cylinder, even if the hysteresis phenomenon and the accompanied discontinuities are absent. The critical flow velocity for which this variation of the vortex mode occurs is close to the resonance velocity.

4.4. Flow Visualization

The first three rows of Figure 6 show the results of flow visualization of the downstream cylinder near-wake, respectively, for $L/D = 7$, 13, and 25, obtained at two reduced velocities; one ($V_r \approx 7$) at or prior to the resonance velocity, and the other ($V_r = 8{\cdot}4$) subsequently to

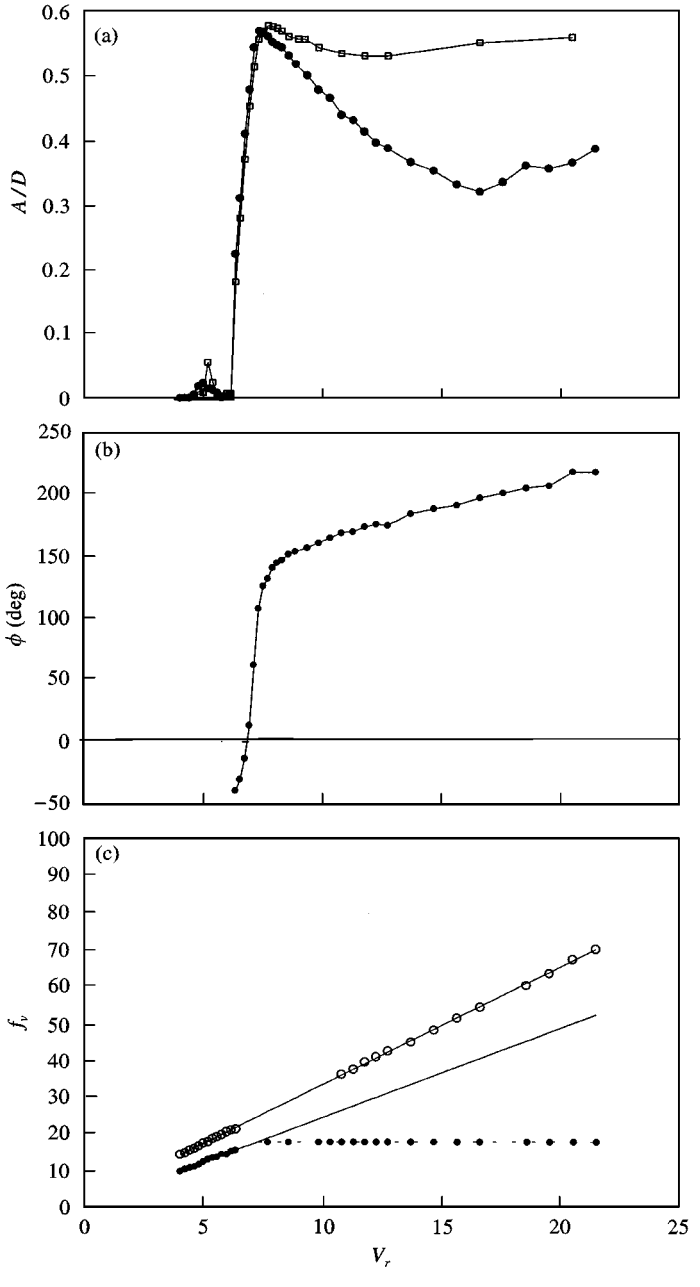

Figure 5. Characteristics of the response of the downstream cylinder at small spacing ratios as a function of the reduced velocity (tandem arrangement, $\alpha = 0°$). (a) A/D: □, $L/D = 7$; ●, $L/D = 8{\cdot}5$: (b) Phase angle Φ: ●, $L/D = 8{\cdot}5$: (c) Vortex-shedding frequency as given by a hot-wire anemometer positioned downstream the rear-cylinder for $L/D = 8{\cdot}5$: ○, f_{v1}; ●, f_{v2}.

the resonance. For comparison, the flow visualization of an isolated cylinder is given in the last row. Before the resonance, the vortices shed from the downstream cylinder are clearly of the 2S type, as shown in Figure 6 (first column). This mode is more regular and less disturbed. Beyond the resonance, the mode of vortex shedding changes, as illustrated in the

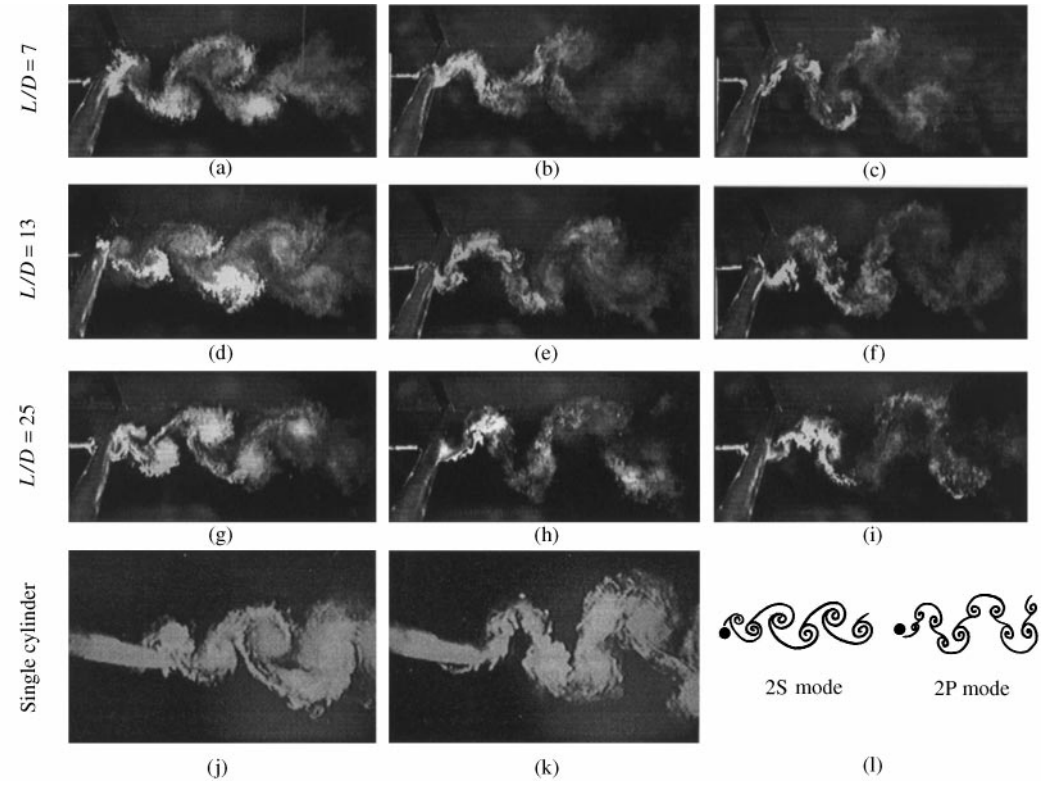

Figure 6. Flow visualization of the downstream cylinder near-wake in comparison with the one of an isolated cylinder. All photographs are taken at the maximum negative displacement of the cylinder. Left column: 2S mode; central and right columns: 2P mode. First row: $L/D = 7$, second row: $L/D = 13$, third row: $L/D = 25$; last row: single cylinder (Brika & Laneville 1993). The first three images of the first row are taken at $V_r = 7$ (g)–7·2 (a, d), the upper six photographs of the second and third rows are taken at $V_r = 8{\cdot}4$ and (j) and (k) at the same velocity $V_r = 5{\cdot}84$; (l) sketches of the 2S and 2P modes.

second and third columns, but its patterns are not as well defined as in the case of an isolated cylinder due the high turbulence of the flow in the wake. This second mode (2P) is also poorly defined because the vortices of each pair have not the same vorticity: the first shed vortex appears stronger than the second, because its vorticity is reinforced by the one of same sign and shed from the corresponding side of the upstream cylinder. The 'eye' of the second vortex is then smaller and less apparent. For more clarity, two pictures of this second mode are given for each separation. As pointed out by Zdravkovich (1982), the visualization also indicates a difference in timing of the shedding of vortices. For the first mode (2S), the vortices are shed from the upper side, while, in the second mode, the vortices are shed from the lower side. This difference in timing which seems to be independent of the separation, characterizes also the 2S and 2P modes observed in the case of a single cylinder. Visualization at $V_r = 16$ showed irregular vortex patterns in the wake of the downstream cylinder.

The vortices shown in Figure 6 are only those shed from the downstream cylinder, but one important aspect of the interference between the cylinders is how these vortices interact with those of the upstream cylinder. The colour picture taken by Kobayashi [see Nakayama (1988)] shows the wakes of two stationary cylinders in tandem arrangement at $L/D = 5$ and $\mathrm{Re} = 10^4$. The vortices shed from each side of the upstream cylinder

reinforce by mixing the ones that are shed from the same side of the downstream cylinder. King & Johns (1976) arrive to the same conclusion with two oscillating cylinders, and their flow visualization showed the vortices shed from the upstream cylinder quickly weakened as they were convected downstream and impinged on the leeward cylinder, even at $L/D = 4$.

In a recent study, Mahir & Rockwell (1996) visualized the flow in the wake of cylinders in tandem ($L/D = 5$, $\mathrm{Re} = 160$) and observed disordered type of modulated response of the wake when both cylinders are stationary. This wake, however, became more regular when the cylinders vibrated. In the synchronization region, locked-on patterns were observed to be stable and insensitive to the value of the phase angle between the displacements of the cylinders.

The absence of the hysteresis loop and the discontinuities in Figure 3 may be interpreted as follows: for the case of an isolated cylinder, the dynamic response is characterized by a hysteresis with two discontinuities, one at an upper critical velocity, which is around the resonance velocity, and the other at a lower critical velocity ($V_r \approx 5{\cdot}5$). The discontinuity in the amplitude A/D at the upper critical velocity is accompanied by a moderate discontinuity in the phase (about 75 deg), while the discontinuity at the lower critical velocity is accompanied by an important variation in Φ (about 180 deg). With the present experimental set-up, no discontinuity has been observed, neither in A/D nor in Φ. The presence of the stationary upstream cylinder that is shedding vortices of the Kármán type (2S mode) seems to prolong the 2S mode of vortex shedding for the downstream cylinder and to retard the appearance of the 2P mode up to V_{res}. On the other hand, if the velocity is progressively reduced from a high value, the second mode of vortex shedding (which is intended to be the 2P mode) appears at high velocities and is maintained until the limit velocity for which the 2S mode is possible is reached. Below this velocity, the second mode of vortices cannot be maintained longer as in the case of an isolated cylinder, and is dislodged by the first mode (2S mode). This dislocation is favoured by the vortices of the upstream cylinder which are of the 2S type. For this reason the hysteresis phenomenon is absent, and the presence of a fixed upstream cylinder leads to a progressive variation in the characteristics of the dynamic response, such as the vibration amplitude, the base pressure, the aerodynamic forces and the phase angle Φ.

The spectra of Figure 7(b, d) show the fundamental frequency f_{v2} with its higher harmonics for velocities $V_r > V_{\mathrm{res}}$, while in those in Figure 7(a, c), for $V_r < V_{\mathrm{res}}$, only the fundamental frequency appears clearly, the amplitude of higher harmonics being very small. A similar difference between the spectra of the hot-wire signal has been noticed in the case of an isolated cylinder (Brika & Laneville, 1995b): the difference between the spectra observed for the same velocity is attributed to the types of the vortex pattern of the cylinder near wake. Higher harmonics are observed in the case of the 2P mode where four vortices are shed per cycle of oscillation. In the case of the present study, the difference between the spectra indicates once again that below and above the resonance velocity two distinct vortex modes exist, as shown in Figure 6: the 2P mode if $V_r > V_{\mathrm{res}}$ and the 2S mode if $V_r < V_{\mathrm{res}}$.

4.5. Comparison with Other Results

4.5.1. V_{res} and the 2S–2P limit curves

Since a definite change in the modes of vortex shedding occurs around the velocity V_{res}, the question arises of its possible link with the critical curve separating the 2S from the 2P modes observed in the case of an isolated cylinder (Williamson & Roshko, 1988). This curve represents the lower limit of the 2P mode (Brika & Laneville 1993). The 2S mode, however,

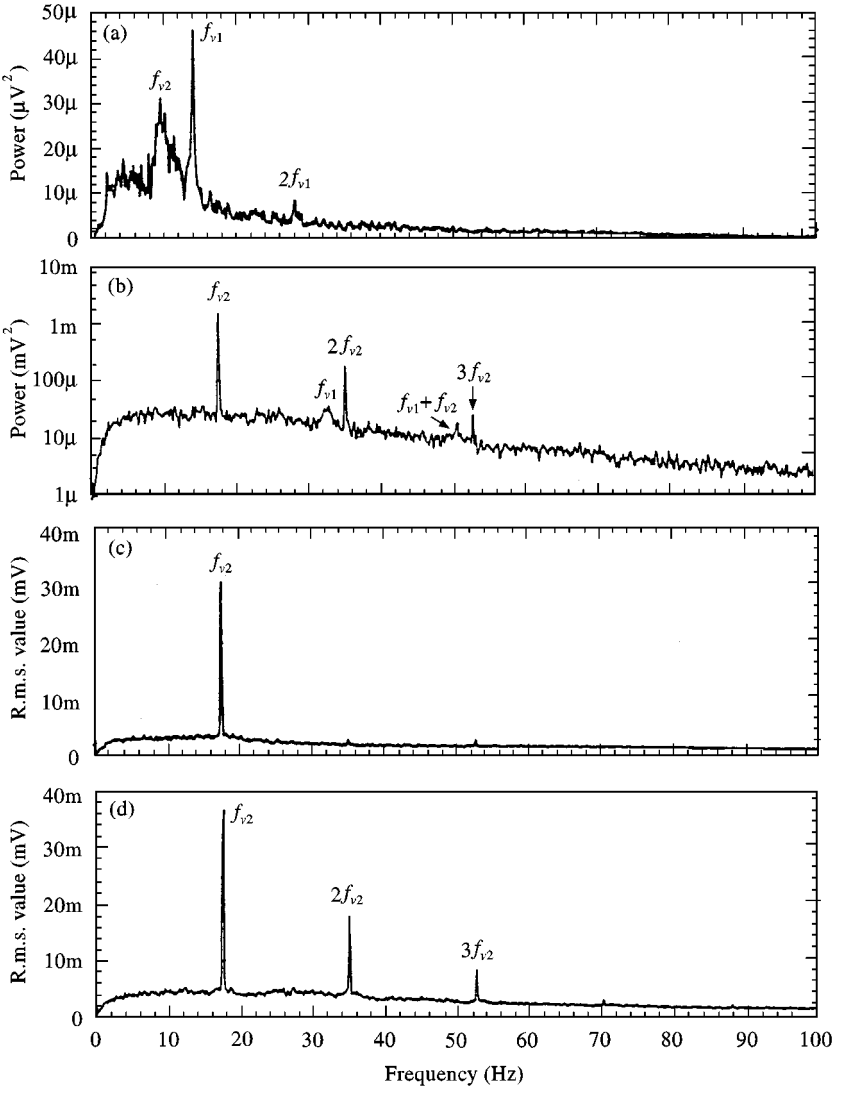

Figure 7. Spectra of the signal of the hot wire anemometer positioned in the wake of the downstream cylinder (tandem arrangement, $\alpha = \beta = 0°$). (a) and (b) $L/D = 8{\cdot}5$ (c) and (d) $L/D = 10$; (a) $V_r = 4{\cdot}2$; (b) $V_r = 9{\cdot}9$; (c) $V_r = 6{\cdot}3$; (d) $V_r = 7{\cdot}4$.

may extend into the 2P mode region and, from the results of Bishop & Hassan (1964), an upper limit of the 2S mode may be deduced.

In a tandem arrangement, the phenomenon presents important dissimilarities: (i) the downstream cylinder oscillates in an unsteady wake; (ii) the switchings from one mode of vortex shedding to another are absent within this unsteady wake.

Nevertheless, the response of the downstream cylinder can be examined in terms of the average velocity in the wake. Figure 8 shows the hot-wire measurements of the mean velocity in the wake centre-line of a stationary cylinder and the mean velocity as estimated from Figure 3(a) by assuming that synchronization onset velocity matches the one of an isolated cylinder ($V_r \approx 5$). The results compare well with those of Norberg (1998) at a similar

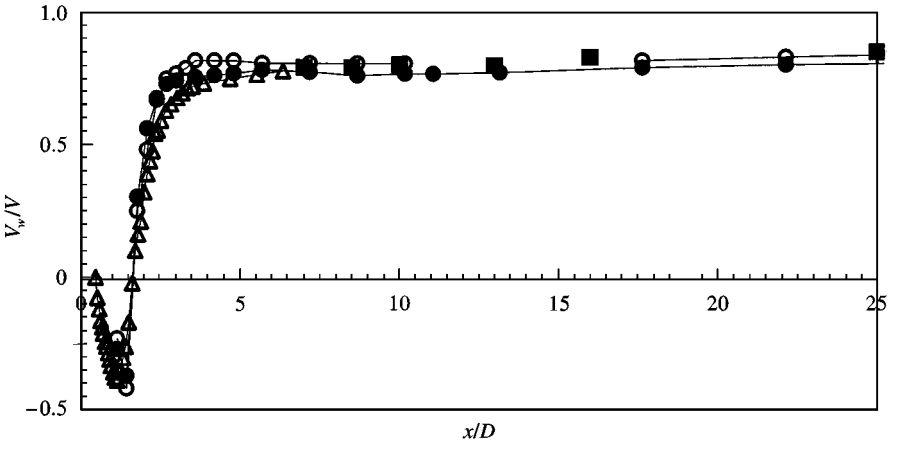

Figure 8. Velocity in the wake of a stationary cylinder. Present study: ■, wake velocity deduced from the velocities at the onset of synchronization; measurements on the wake centre-line: ○, $V_r = 6{\cdot}0$ (Re = 7700); ●, $V_r = 8{\cdot}3$ (Re = 8100); △, Norberg (1998) Re = 8000.

Reynolds number. Figure 9 presents the response of the downstream cylinder† as a function of the reduced wake velocity. As L/D increases, the response tends to the one of an isolated cylinder. When the limit curves of the 2P and 2S modes are superimposed, one can deduce that, within experimental precision, V_{res}, in all cases studied, is fairly close to the critical curve of Bishop & Hassan (1964) (upper limit of the 2S mode).

4.5.2. Wake interference galloping

In order to examine the wake interference galloping, the results of the present study at $L/D = 7$ and $8{\cdot}5$ are compared with some results of King & Johns (1976) and Ruscheweyh (1983). The results cannot, however, be compared directly since they have been obtained with flexible models vibrating in different mode shapes. The models used by Ruscheweyh and King & Johns are cantilevered cylinders vibrating in their first mode, while in the present study the cylinder vibrates in its first free–free mode. To take into account the mode shape, the normalized amplitude $A/\gamma D$ is used rather than A/D, γ being the mode shape factor defined as (Blevins 1990),

$$\gamma = y_{max}\left[\frac{\int_0^l y^2(z)\,dz}{\int_0^l y^4(z)\,dz}\right]^{1/2} = \left[\frac{\int_0^1 (y^2(z/l)/y_{max}^2)\,(dz/l)}{\int_0^1 (y^4(z/l)/y_{max}^4)\,(dz/l)}\right]^{1/2}, \tag{1}$$

where $y(z)$ is the cylinder displacement at the spanwise position z from one end (the clamped end in the case of the cantilevered cylinder) and y_{max} is the maximum amplitude of the mode shape.

For a cantilevered cylinder vibrating in its first mode, we get $\gamma = 1{\cdot}305$, while for the first free–free vibration mode, we get $\gamma = 1{\cdot}47$. For the present study, however, only the part between the nodes of the first mode is exposed to flow. This part has a factor $\gamma = 1{\cdot}15$ which is approximately equal to that of a sinusoidal mode shape ($\gamma = 1{\cdot}155$) since the exposed part oscillates with a quasi-sinusoidal form. Since $\gamma = 1{\cdot}0$ for a rigid cylinder, the normalized amplitude can be considered as the one of a rigid cylinder.

† The amplitudes of Figure 9 are normalized, as explained in Section 4.5.2.

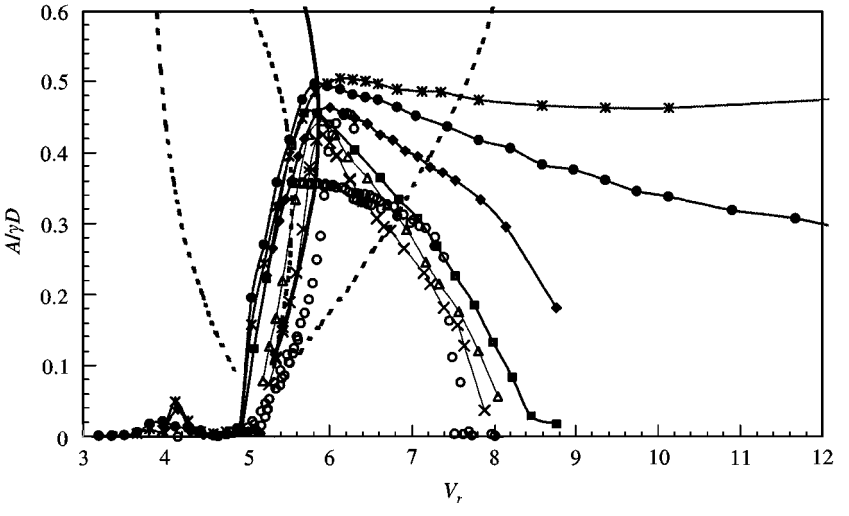

Figure 9. Present results corrected for the shielding effect and the mode shape in comparison with other results. *, $L/D = 7$; ●, $L/D = 8{\cdot}5$; ◆, 10; ■, $L/D = 13$; △, $L/D = 16$; X, $L/D = 25$; ○, single cylinder; —, Bishop & Hassan (1964); - - - -, Williamson & Roshko (1988).

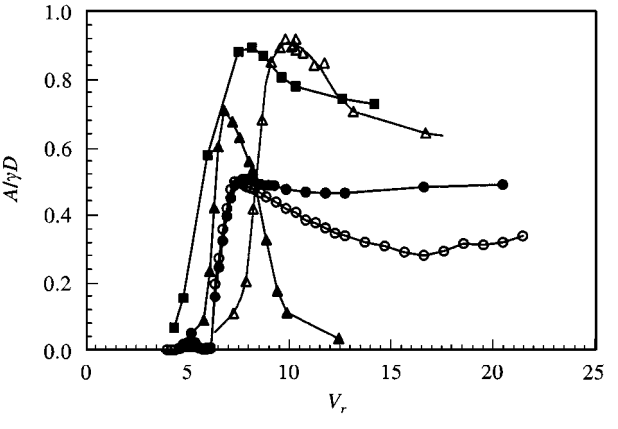

Figure 10. Comparison between the normalized amplitude of the present study and those of King & Johns (1976) and Ruscheweyh (1983). King & Johns: ■, $L/D = 5{\cdot}5$, $\beta = 0°$, Sc = 0·5. Ruscheweyh: △, $L/D = 4{\cdot}8$, $\alpha = 0°$, $\beta = 5°$, Sc = 1·6; ▲, $L/D = 7{\cdot}3$, $\beta = 10°$, Sc = 1·5. Present study ($\alpha = \beta = 0°$, Sc = 4·1 at maximum amplitude): ●, $L/D = 7$; ○, $L/D = 8{\cdot}5$.

The comparison between the normalized amplitudes is shown in Figure 10. As in the case of the present study, both the results of King & Johns at $L/D = 5{\cdot}5$ and Ruscheweyh at $L/D = 4{\cdot}8$ show a similar behaviour as in the present results: a slight decrease of the amplitude of vibration beyond the value of V_r at which the maximum occurs and vibrations at higher reduced velocity well beyond the end of synchronization of a single cylinder. Noting that, in the experiments of King & Johns and Ruscheweyh, both the upstream and downstream cylinders are free-vibrating and the upstream cylinder comes to rest around $V_r = 8{\cdot}5$. The results also indicate that the synchronization onset velocity of the downstream cylinder is higher than that of a single cylinder due to the reduction of the mean velocity in the wake of the upstream cylinder. At $L/D \approx 5$, the mean velocity in the wake of

the upstream cylinder is lower than at $L/D = 7$, the onset of synchronization and the maximum amplitude then occur at higher reduced velocities as indicated by Ruscheweyh's results (open triangles).

The results of King and Johns conducted in a water channel at $L/D = 4{\cdot}8$ are, however, shifted to the left. The difference between the maximum amplitudes of the different tests is attributed to the effects of the Scruton number (see the caption) and L/D, as shown in Figure 3. On the other hand, the Scruton number in both results of Ruscheweyh (full triangles, $L/D = 7{\cdot}3$; and open triangles, $L/D = 4{\cdot}8$) is almost the same (1·5–1·6), but the maximum amplitude is significantly reduced, indicating then that the effect of L/D is the most important.

For $L/D \approx 7$, the results of Ruscheweyh (full triangles) indicate that V_{res} and the onset of synchronization are in good agreement with those of the present study. The difference in the maximum amplitude is due to the difference in the Scruton number (1.5 relative to 4.1). Ruscheweyh's data at $L/D = 7{\cdot}3$ show, however, that the cylinder comes to rest around $V_r = 12$: this can be explained by the fact that the cylinders in Ruscheweyh's experiments are not in a tandem arrangement, but they are staggered at $\beta = 10^\circ$. As will be discussed in the next section, the stagger angle has a great effect on the synchronization range and, at this particular value of β, the wake interference is significantly reduced and the downstream cylinder response is nearly similar to that of an isolated cylinder.

5. STAGGERED ARRANGEMENT

5.1. Dynamic Response

Figure 11 shows the effect of the bundle inclination angle β on the dynamic response of the leeward cylinder for different planes of vibration and a separation of $L/D = 13$, typical of bundles of high voltage transmission lines. The results of this figure indicate that an increase in the angle β reduces the synchronization region, the synchronization onset velocity and, to a certain degree, the maximum amplitude of oscillation. The hysteresis phenomenon and the associated discontinuities observed in the response of an isolated cylinder begin to appear progressively once again with an increasing value of β. For a bundle inclination angle $\beta = 20^\circ$, the dynamic response of the leeward cylinder is similar to that of a single cylinder. This indicates that, beyond $\beta = 20^\circ$, the rear cylinder is outside the wake of the fixed upstream cylinder and therefore behaves as an isolated one. Pon *et al.* (1989) also observed that, for $L/D = 15$, the downstream cylinder behaves like a single cylinder when the bundle is oriented at angles of $\beta \geq 20^\circ$.

Figure 12 shows traces of the downstream cylinder displacement and the phase angle Φ between the vortex shedding from this cylinder and its displacement. The traces in Figure 12(a, b) display the sudden jumps in the vibration amplitude at $\beta = 15^\circ$, and in Figure 12(c, d) for $\beta = 20^\circ$ they show a slow increase and decrease of flow velocity. They all indicate an abrupt change in the amplitude, accompanied by a similar variation in the phase angle Φ. In traces (a), V_r is slowly increased from 6·22 to 6·28, while in traces (b), V_r is decreased from 6·28 to 6·22 showing no hysteresis phenomenon with a double amplitude region. Traces of Φ are more fluctuating at $V_r = 6{\cdot}22$ than at $V_r = 6{\cdot}28$. Traces in the case of an isolated cylinder (Brika and Laneville 1993) showed a similar behaviour; less fluctuations in Φ are observed when the wake vortex pattern is of the 2P type and the opposite when the vortices are of the 2S type. This confirms again that, beyond the resonance velocity, a second vortex mode exists and is different from a first one present below the resonance velocity as shown in Figure 6. Moreover, a "kink" may be observed in the dynamic response of the downstream cylinder, just to the right of the resonance [see for example Figure 11(a)].

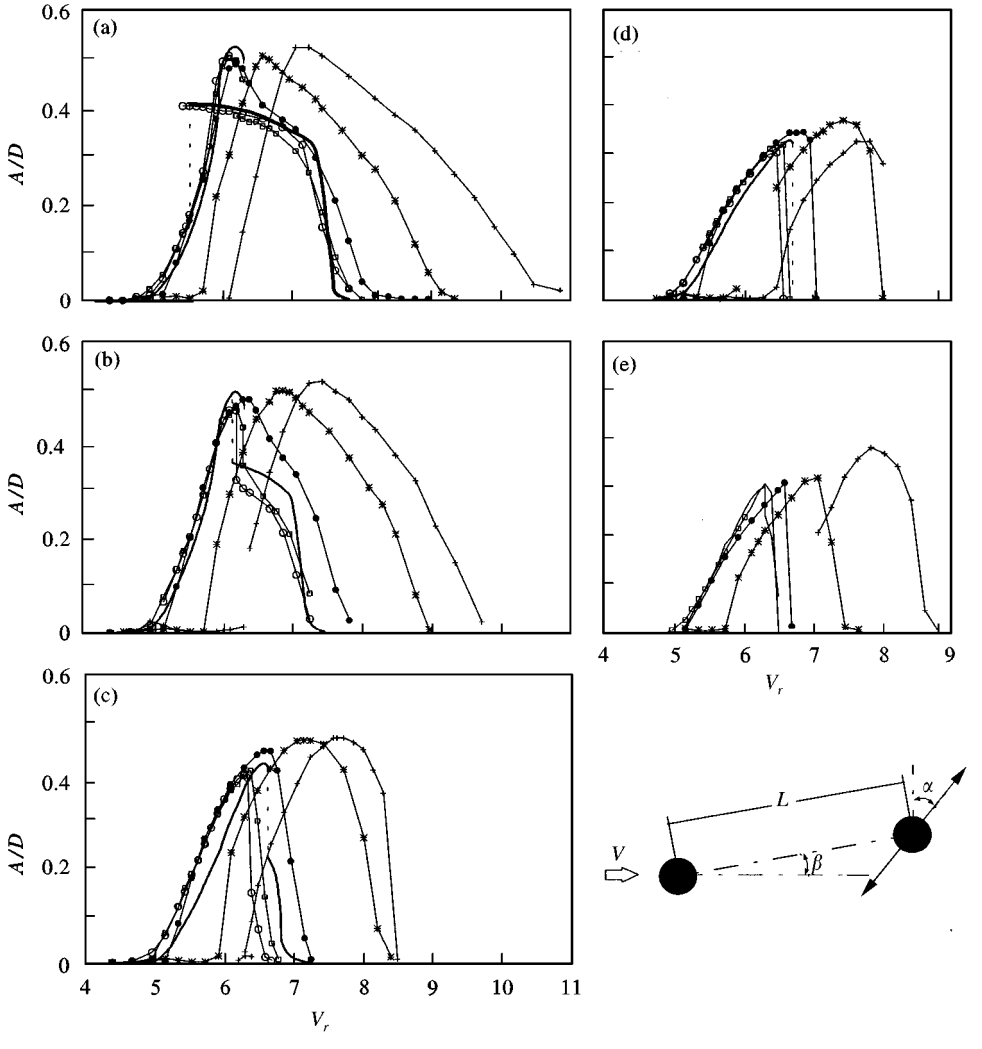

Figure 11. Effect, for different planes of vibration, of the stagger angle β on the response of the downstream cylinder ($L/D = 13$): (a) $\alpha = 0°$; (b) $\alpha = 15°$; (c) $\alpha = 30°$; (d) $\alpha = 45°$; (e) $\alpha = -45°$. +, $\beta = 0°$; *, $\beta = 5°$; ●, $\beta = 10°$, □, $\beta = 15°$; ○, $\beta = 20°$; —, single cylinder.

This kink is more obvious at higher values of β than at lower ones and, for $\beta \geq 20°$, the kink becomes a clear discontinuity as in the case of an isolated cylinder.

Traces in Figure 12(c) for $\beta = 20°$ show an instantaneous discontinuity in both displacement and Φ occurring when V_r is slowly increased from 6·22 to 6·28 as in the previous case of $\beta = 15°$ and the case of an isolated cylinder. For a decreasing velocity, however, the abrupt change in Φ and A does not occur between $V_r = 6{\cdot}28$ and 6·22 as in the previous case, but at a smaller value when V_r is slowly decreased from 5·53 to 5·47, as shown in Figure 12(d). A similar discontinuity at $V_r = 5{\cdot}47$ is also observed with a single cylinder showing that, beyond $\beta = 20°$, the downstream cylinder is outside the wake of the fixed upstream cylinder.

Figure 13 shows the effect of α and β on the variation, as a function of V_r, of the phase Φ between the vortex shedding of the downstream cylinder and its displacement. For $\alpha = 0°$ and $\beta = 5°$, the phase Φ increases rapidly with V_r between the velocity for the onset of

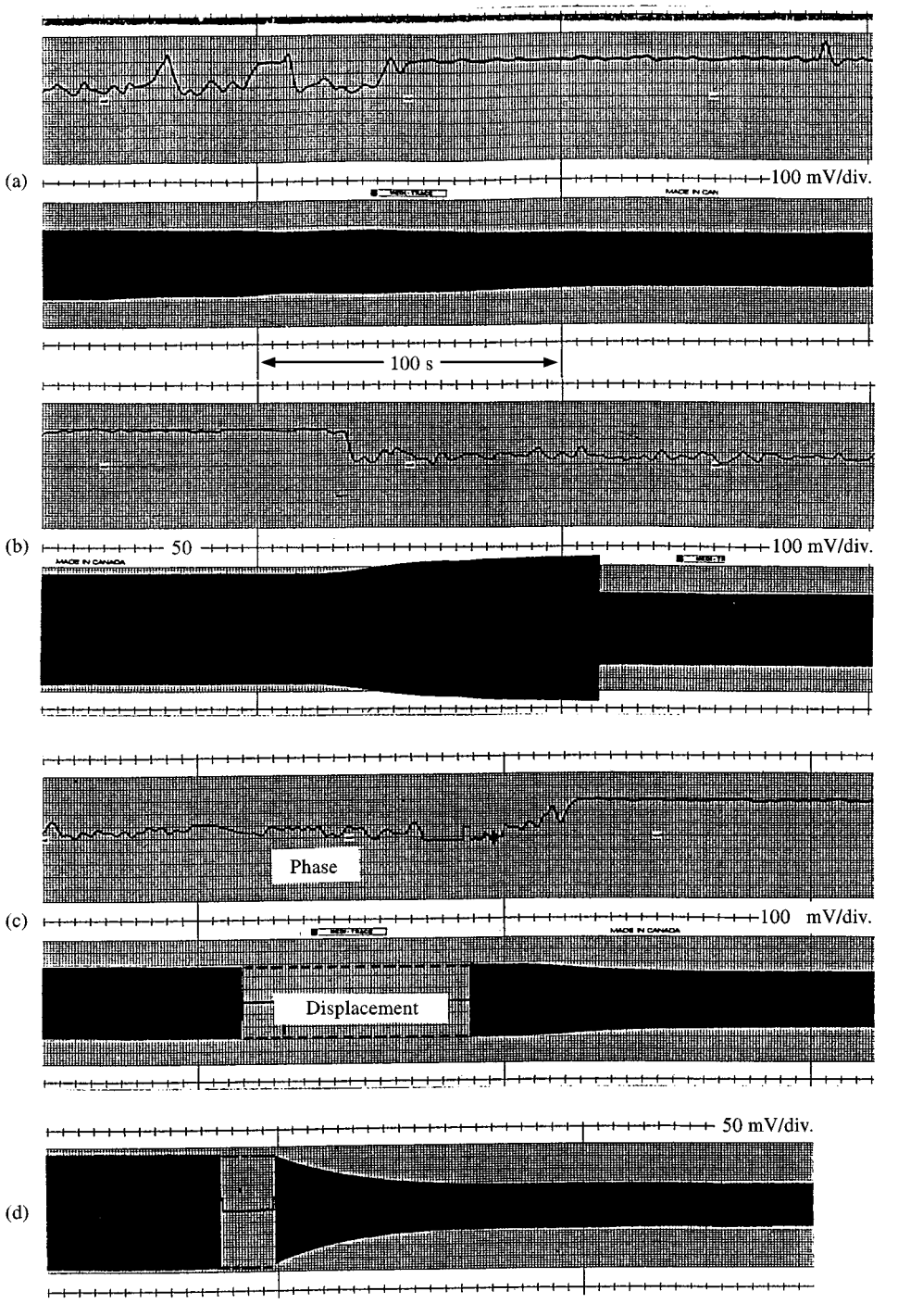

Figure 12. Traces of the cylinder displacement and phase angle Φ showing the discontinuities at the upper and lower critical velocities for (a, b) $\beta = 15^\circ$ and (c, d) $\beta = 20^\circ$ (a) Reduced velocity V_r slowly increased from 6·22 to 6·28; (b) V_r decreased from 6·28 to 6·22; (c) V_r increased from 6·22 to 6·28; (d) V_r decreased from 5·53 to 5·47.

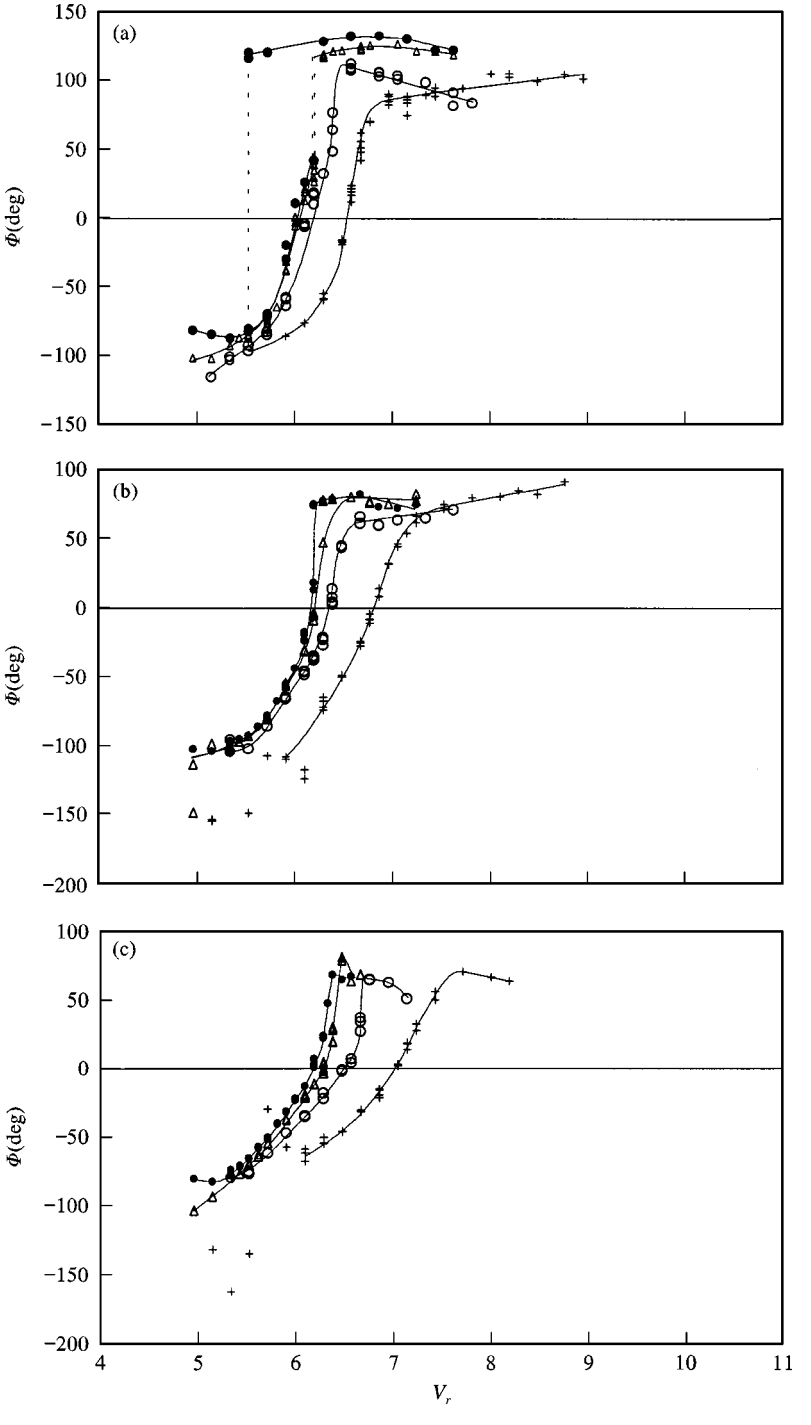

Figure 13. Effect, for different planes of vibration, of the stagger angle β on the phase angle Φ between the vortex shedding and the displacement of the downstream cylinder ($L/D = 13$): (a) $\alpha = 0°$; (b) $\alpha = 15°$; (c) $\alpha = 30°$. +, $\beta = 5°$; ○, $\beta = 10°$; △, $\beta = 15°$; ●, $\beta = 20°$.

synchronization and the resonance velocity at which maximum amplitude occurs (see Figure 11). Beyond the resonance velocity, the curve of the phase data flattens and Φ increases gradually with V_r, indicating a possible change of the vortex pattern in the wake of the downstream cylinder, as discussed before for the case ($L/D = 8{\cdot}5$, $\alpha = 0^\circ$, $\beta = 0^\circ$). As the bundle inclination angle, β, is increased, the curve of the phase angle shifts towards the left and tends progressively to that of an isolated cylinder. The shift is more pronounced at smaller values of β than at higher values. This is attributed to the profile of the mean velocity in the wake of a fixed cylinder. Around the resonance velocity, the phase change between the modes of vortex shedding occurs in a more drastic manner as β is increased, leading to the appearance of a discontinuity in the characteristics of the downstream cylinder response. For $\beta = 20^\circ$, the curve of the phase angle is similar to the one of an isolated cylinder with the hysteresis phenomenon for $\alpha = 0$ and 15° and the associated discontinuities. The results of the phase angle prove once again the presence of two modes of vortex shedding in the wake of the downstream cylinder, essentially the 2S and 2P modes as in the case of an isolated cylinder, in spite of the absence of the hysteresis phenomenon and the discontinuities in the dynamic response of this cylinder when it is submerged in the wake of the fixed upstream cylinder. The 2S mode ceases to exist beyond the resonance velocity in all cases, for an isolated cylinder as well as for the configuration of the present experimental set-up.

5.2. Bifurcation Phenomenon

Figures 14 and 15 show typical traces, for two different velocities and the stagger angle $\beta = 15^\circ$ ($\alpha = 0^\circ$ and $L/D = 13$), of the time variation of Φ and A when the vibrating model is released from rest and from a high amplitude initially pumped up with a shaker. For each value of V_r, the vibration amplitude A/D as a function of time for these two cases is also represented on a same graph. For a better comprehension of these figures, some results observed in the case of an isolated cylinder under similar initial conditions are repeated. When the cylinder is released from rest at $V_r > 5{\cdot}5$, its steady state amplitude is always the one associated with the 2P mode. When it is released from a high amplitude, its displacement stabilizes either on the curve associated with the 2S mode (C2S) or on that of the 2P mode (C2P). The probability that it stabilizes on the C2S decreases with increasing value of V_r and, beyond $V_r = 6{\cdot}0$, it can only stabilize on the C2P curve (Brika & Laneville 1993).

In the present study ($\beta = 15^\circ$), a relatively different behaviour is observed in the probability of existence of the 2S mode at high velocities. The results of Figure 14 obtained at $V_r = 5{\cdot}9$ indicate that, when the model is released from rest, the amplitude increases and tends to stabilize on the C2P curve; then it suddenly bifurcates and keeps on increasing to stabilize finally on the C2S curve. This bifurcation is accompanied by a sudden change of the phase angle Φ. When the model is released from a high amplitude, it stabilizes directly on the C2S without any discontinuity in Φ and A [see Figure 14(b)]. Figure 15 is obtained for $V_r = 6{\cdot}3$, a velocity that is around the resonance and corresponds to the higher velocity for which the 2S mode may exist. The figure shows that, when the model is released from rest, it stabilizes on the C2P curve and maintains this steady state amplitude. If the cylinder is released from a high amplitude, the cylinder displacement and the phase Φ display two different discontinuities; the first may be attributed to a sudden switch from mode 2P to mode 2S, and the second from 2S to 2P. The phase Φ for the 2P mode being more constant and the fluctuations appearing in Φ indicate a competition between the two modes of vortex shedding. To summarize the results of Figures 14 and 15, it can be said that the vortices of the Kármán-type shed from the fixed upstream cylinder help in the establishment of the

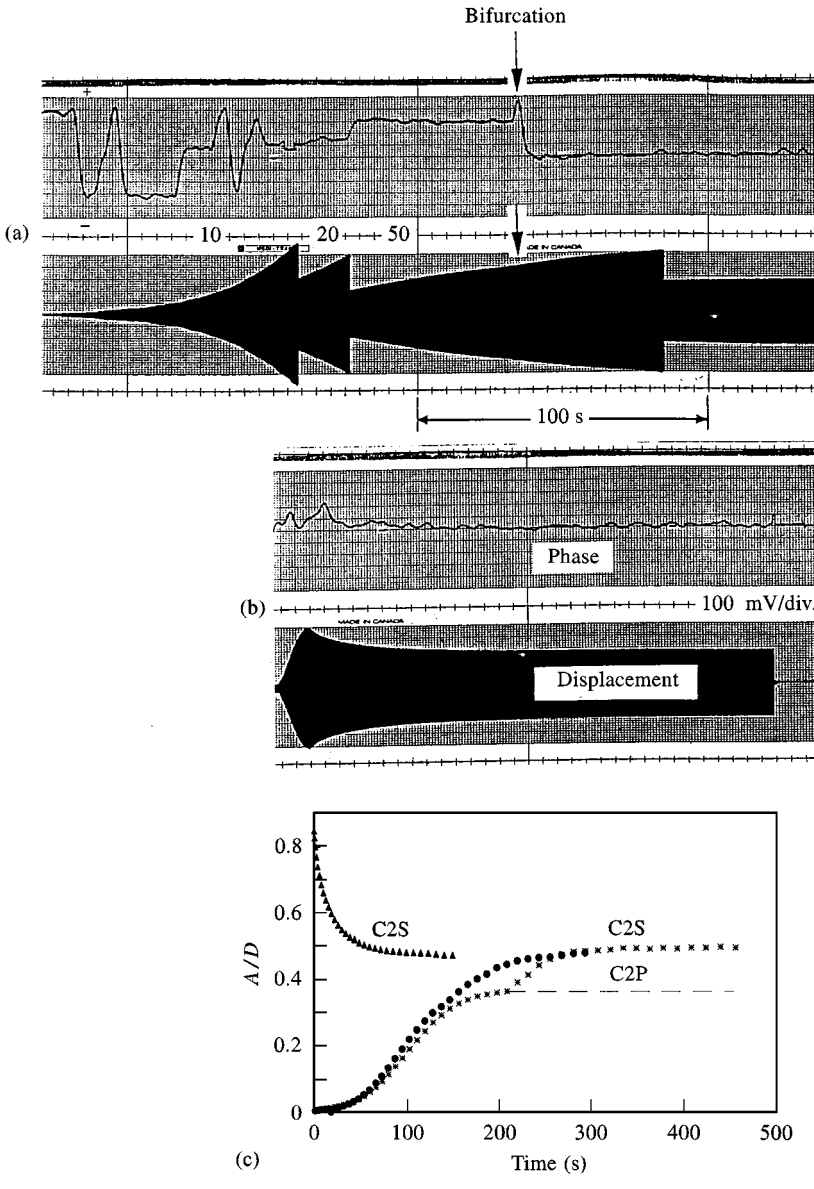

Figure 14. The vibration amplitude and phase angle Φ as a function of time ($L/D = 13$, $\alpha = 0°$, $\beta = 15°$, $V_r = 5{\cdot}9$), (a) from rest, (b) from a high amplitude, (c) A/D versus time: *, from rest (trace a); ●, from rest; △, from a high amplitude (trace b); - - - -, steady state amplitude of the 2P mode.

2S mode and increase its probability of existence at high velocities. Beyond the resonance, only the second mode (2P) exists as shown in Figure 16.

For larger values of angle β, say $\beta = 20°$, such a bifurcation is also present, but it occurs at lower flow velocities. Figure 17 shows the records obtained for a reduced velocity of $V_r = 5{\cdot}5$ and the case ($L/D = 13$, $\alpha = 0°$ and $\beta = 20°$) as the model is released from rest and from a high amplitude of excitation. The traces contain bifurcations occurring at different amplitudes for the same flow velocity. Each bifurcation is again accompanied by a sudden

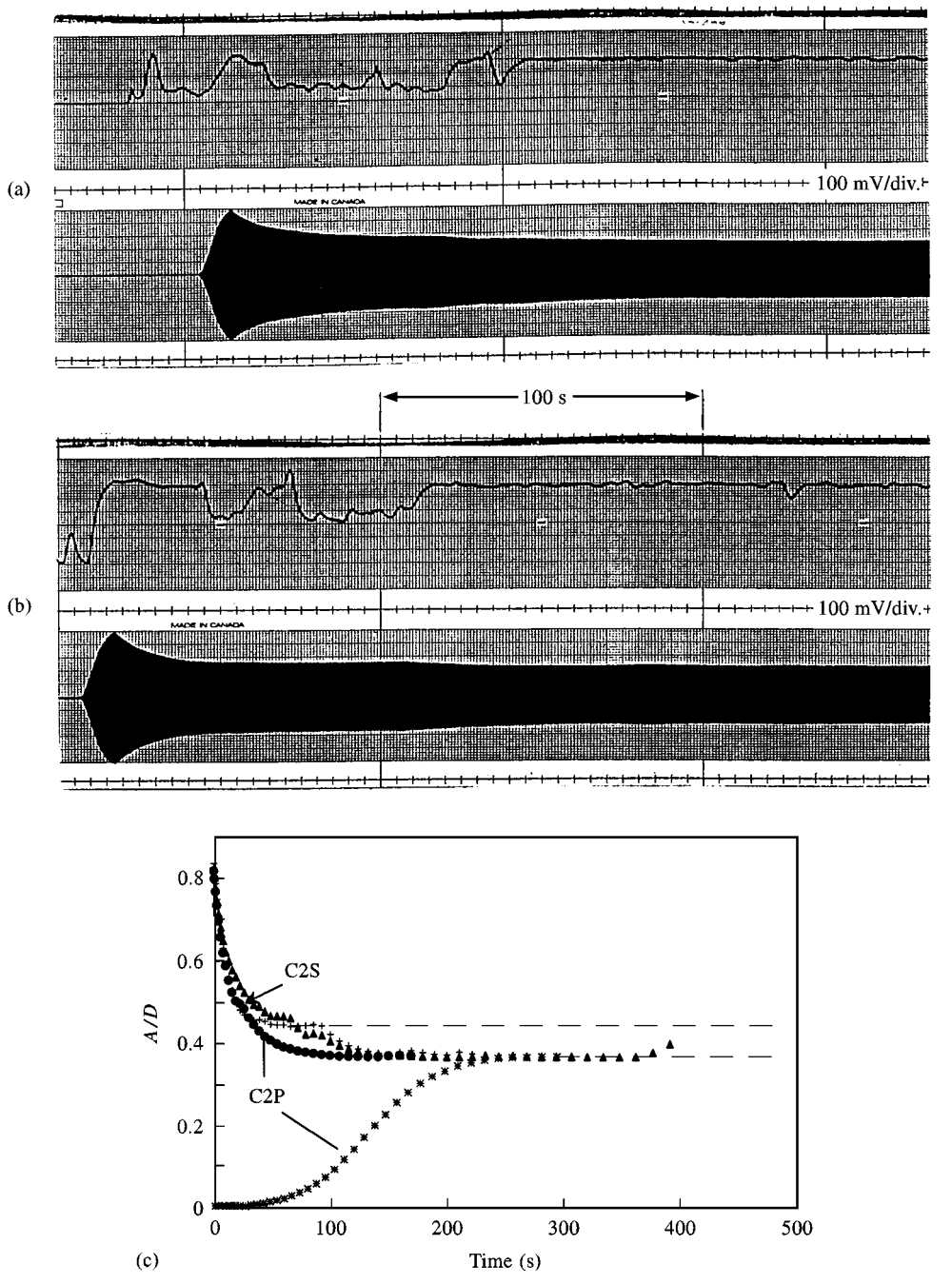

Figure 15. The vibration amplitude and phase angle Φ as a function of time ($L/D = 13$, $\alpha = 0°$, $\beta = 15°$, $V_r = 6{\cdot}3$). (a) and (b) from a high amplitude; (c) A/D versus time: *, from rest; ●, from a high amplitude; ▲, from a high amplitude (trace a); +, from a high amplitude (trace b).

change of the phase angle Φ, indicating an instantaneous change in the wake vortex patterns of the downstream cylinder.

For the different planes of vibration, the bifurcation amplitudes of the downstream cylinder are presented in Figure 18 for $\beta = 15$ and $20°$ in comparison with the results of

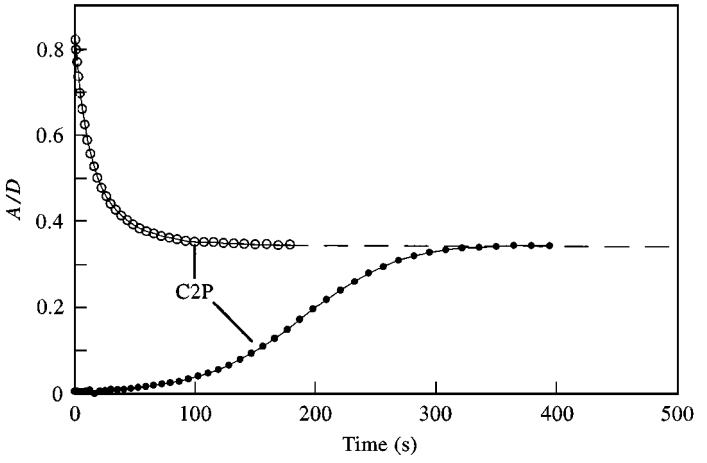

Figure 16. The vibration amplitude as a function of time ($L/D = 13$, $\alpha = 0°$, $\beta = 15°$, $V_r = 6{\cdot}7$): ●, from rest; ○, from a high amplitude.

Williamson & Roshko (1988) and the bifurcation amplitudes of an isolated cylinder as obtained by Brika & Laneville (1995a). To take account of the vibration mode shape, the amplitude presented in Figure 18 is the normalized one. It is worthwhile to notice here that the results of the present study are obtained with a free vibrating cylinder while those of Williamson & Roshko (W&R) are obtained with a forced-oscillating cylinder at lower Reynolds numbers ($300 < \mathrm{Re} < 1000$). Parkinson (1989) discussed in detail the similarities and dissimilarities between the two approaches. The map of vortex patterns given in figure 3 of W&R is the baseground of the present comparison, and it is assumed "representative of those patterns to be found over a large range of Re" as mentioned by W&R. Zdero *et al.* (1995), in a limited study ($A/D = 1$ and 3·5, $\mathrm{Re} = 2000$) confirmed the patterns of W&R, showing that the boundaries of the 2P mode at $A/D = 1$ are not greatly affected. The experimental results of Brika & Laneville (1993), conducted in similar conditions as in the present study, confirmed the critical curve separating the 2S and 2P regions.

For a vibration orthogonal to the flow direction ($\alpha = 0°$), Figure 18(a) indicates that for the bundle orientation $\beta = 15°$, the switch from the 2P mode to the 2S mode occurs at much higher velocities than for $\beta = 20°$. In other words, at the same reduced velocity, the switch occurs at earlier stages of the time history of the cylinder motion from rest. For $\beta = 15°$, the bifurcation amplitude curve is in the middle of the 2P mode region, while, for $\beta = 20°$, it becomes closer to the critical curve separating the 2P and 2S mode regions (W&R). For this last angle value, the bifurcation amplitude curve coincides with the one of an isolated cylinder confirming, once again that beyond $\beta = 20°$, the downstream cylinder is outside the upstream cylinder wake and behaves as an isolated one.

For the other planes of vibration, the same tendency is respected. Thus, for a given inclination of the same plane of vibration and flow velocity, the bifurcation occurs at lower amplitudes for $\beta = 15°$ than for $\beta = 20°$. Beyond this last stagger angle, the bifurcation amplitude curve tends to that of an isolated cylinder, as measured by Brika & Laneville (1995a). This may be explained as follows: at $\beta = 15°$, the downstream cylinder is initially outside or on the boundary of the wake of the upstream cylinder when it is released from rest. Accordingly, it behaves as a single cylinder for which the wake vortex pattern is of the

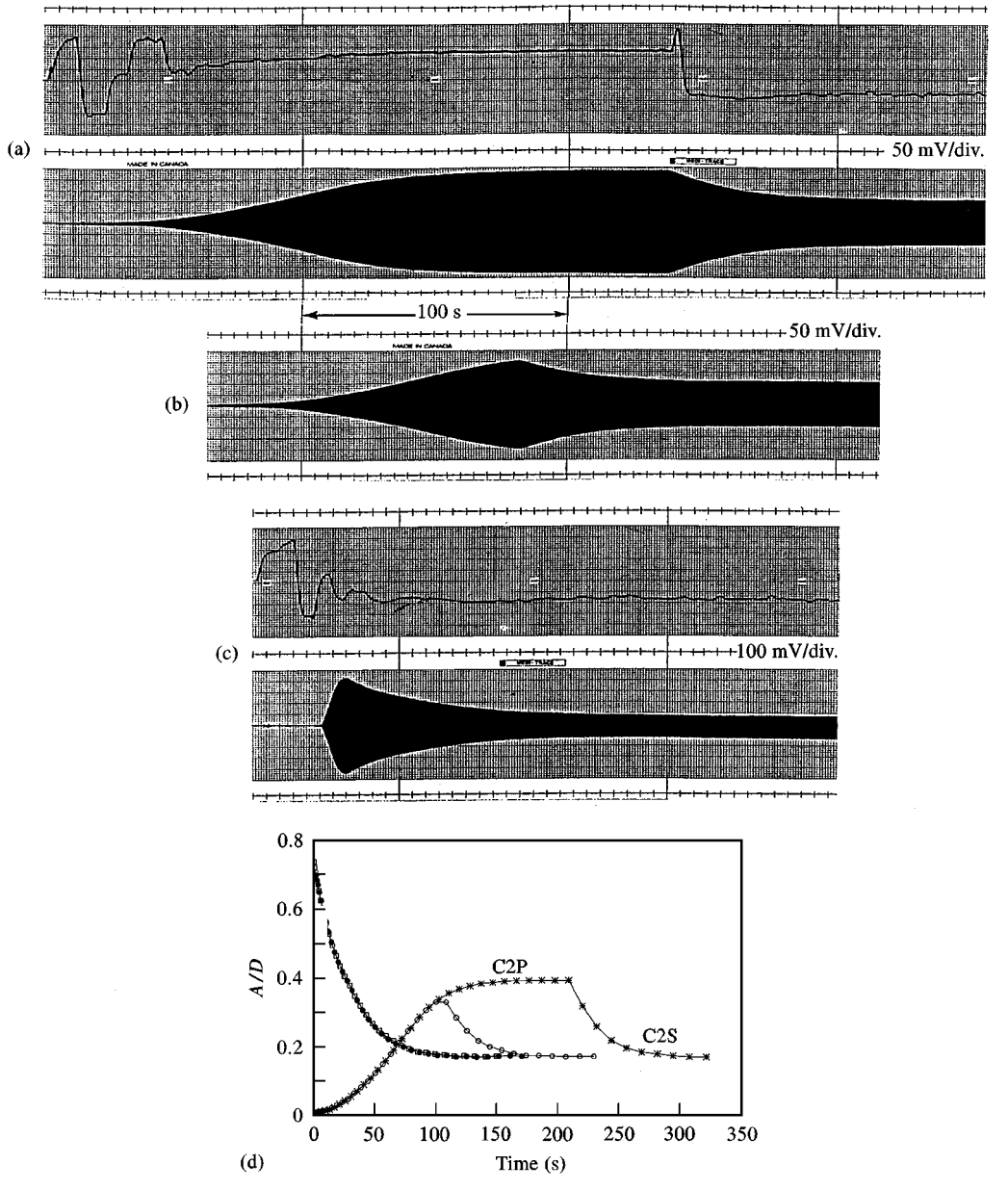

Figure 17. The vibration amplitude and phase angle Φ as a function of time ($L/D = 13$, $\alpha = 0°$, $\beta = 20°$, $V_r = 5{\cdot}5$). (a) and (b) from rest; (c) from a high amplitude; (d) A/D versus time: *, from rest (trace a); ○, from rest (trace b); ●, from a high amplitude (trace c); □, from a high amplitude.

2P type (Brika & Laneville 1993). As its amplitude grows, it penetrates progressively in the wake of the windward cylinder that contains vortices of the 2S type (natural Kármán vortices). Once immersed in this wake, its own wake vortex pattern changes from the 2P mode to the 2S mode, accompanied by a bifurcation in its amplitude and a sudden change of the phase Φ between the vortex shedding and the cylinder displacement, as shown in Figure 14(a).

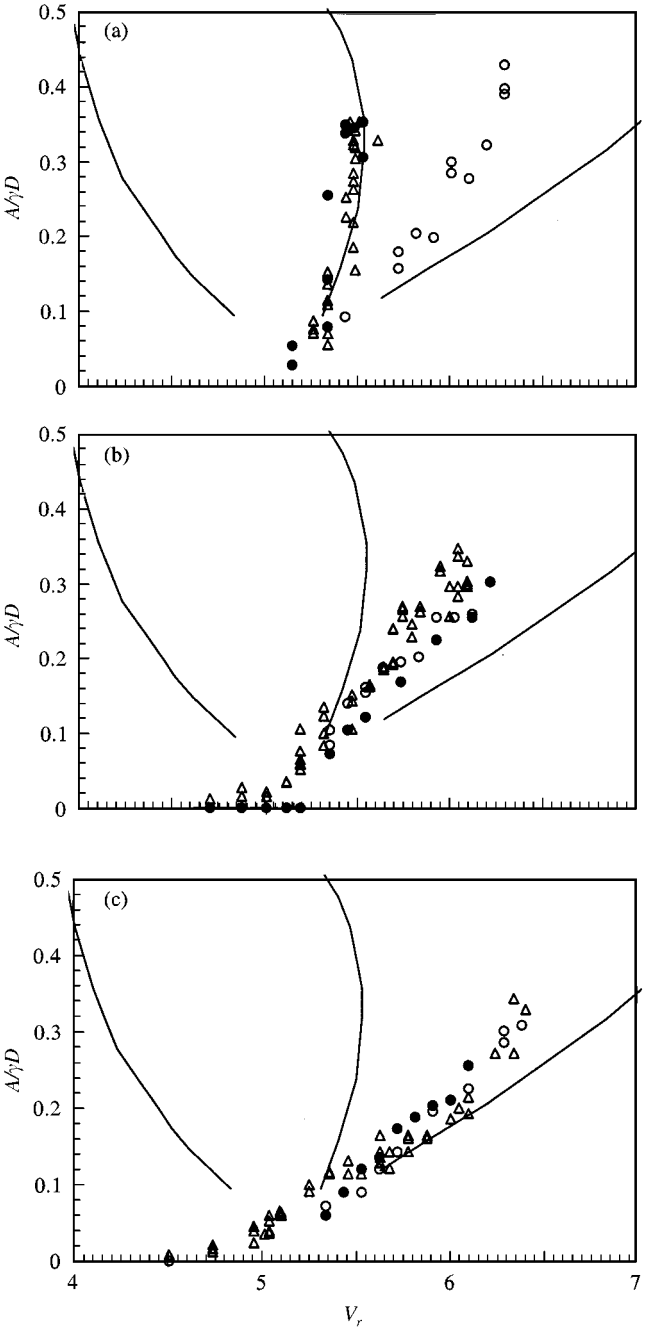

Figure 18. Comparison between the results of Williamson & Roshko (1988) and the effect of the stagger angle β on the normalized amplitude of bifurcation obtained with the present set-up: (a) $\alpha = 0°$; (b), $\alpha = 15°$; (c), $\alpha = 30°$. ●, $\beta = 15°$; ○, $\beta = 20°$; △, single cylinder; —, Williamson & Roshko.

6. EFFECT OF α

Figure 19 shows the effect of the plane of vibration, α, on the dynamic response of the downstream cylinder for the different separations, L/D, studied when the cylinders are in

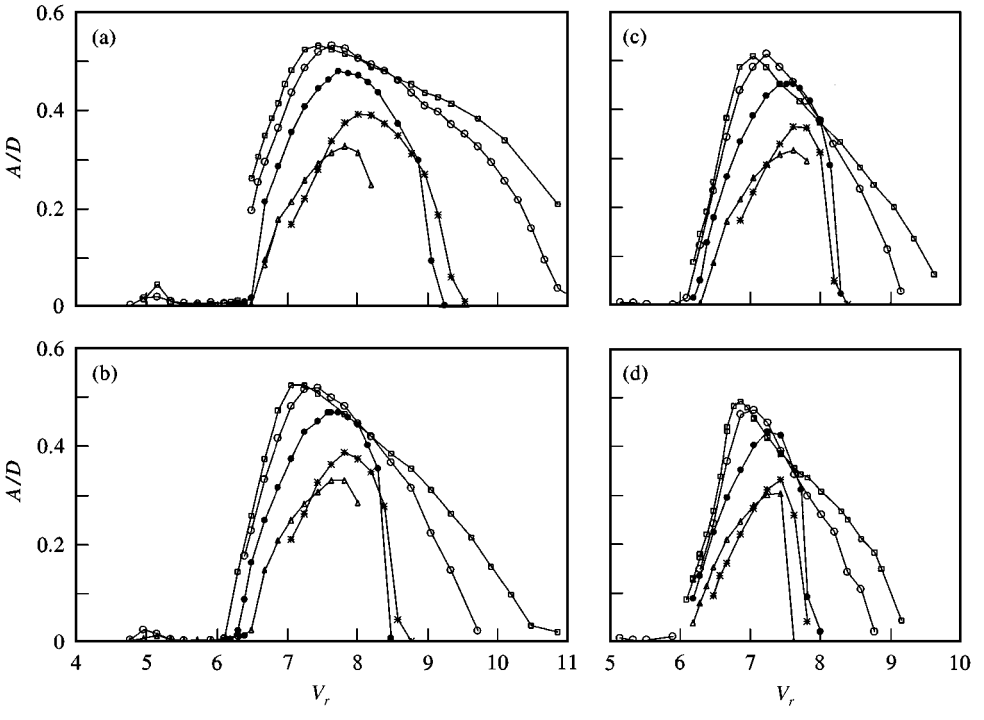

Figure 19. Effect, for different L/D separations in the tandem arrangement, of the plane of vibration on the response of the downstream cylinder: (a) $L/D = 10$; (b) 13; (c) 16; (d) 25. □, $\alpha = 0°$; ○, $\alpha = 15°$; ●, $\alpha = 30°$; △, $\alpha = 45°$; *, $\alpha = -45°$.

tandem. The results of this figure indicate that, for all values of L/D, an increase of angle α: (i) reduces the maximum amplitude of vibration and the synchronization region and (ii) increases the resonance velocity as well as the synchronization onset velocity. The first three effects are similar to those observed with an isolated cylinder vibrating in different incident planes (Brika & Laneville 1995a).

When the cylinders are in a staggered arrangement with $L/D = 13$, the effect of the angle α is shown in Figure 20 for different bundle inclinations. For $\beta \geq 5°$, the onset of synchronization seems to occur at the same reduced velocity for all vibration planes. This synchronization onset velocity decreases with increasing β. For increasing α, as observed in the case of an isolated cylinder (Brika & Laneville 1995a), the resonance velocity increases and the maximum amplitude as well as the velocity of the end of synchronization decrease with α for each bundle inclination angle. For both planes $\alpha = 45°$ and $-45°$, the vibration amplitude seems to be slightly different at the same reduced velocity. The velocity of the end of synchronization does not match in this case.

7. CONCLUSIONS

The conclusions of an experimental investigation of vortex-induced vibrations of a lightly damped flexible cylinder vibrating in different planes in the wake of a fixed cylinder can be summarized as follows.

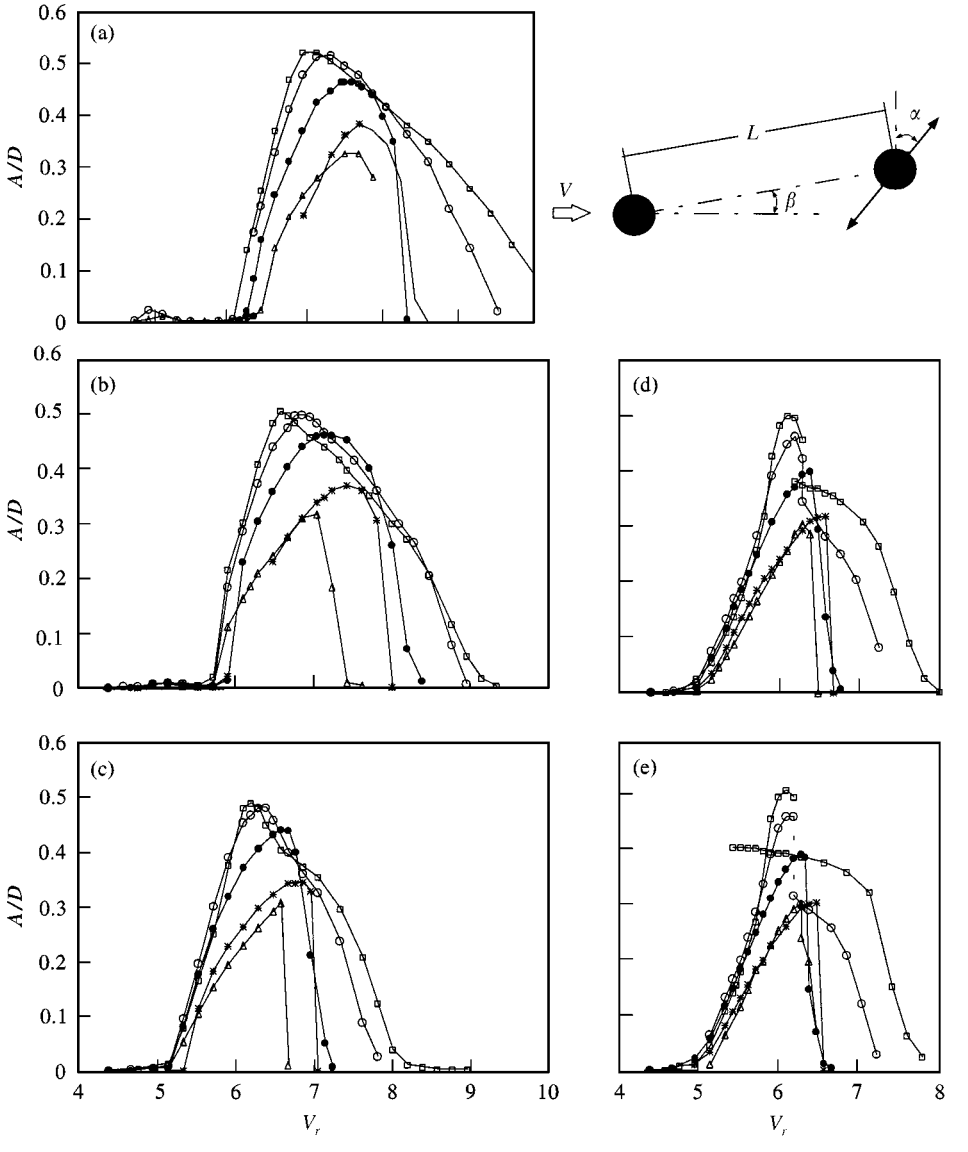

Figure 20. Effect, for different stagger angles β, of the plane of vibration on the response of the downstream cylinder at $L/D = 13$ (a), $\beta = 0°$; (b) $\beta = 5°$; (c) $\beta = 10°$; (d) $\beta = 15°$; (e) $\beta = 20°$. □, $\alpha = 0°$; ○, $\alpha = 15°$; ●, $\alpha = 30°$; △, $\alpha = 45°$; *, $\alpha = -45°$.

(a) In a tandem arrangement with $7 < L/D < 25$, the downstream cylinder response is not hysteretic; the onset of synchronization occurs at an undisturbed flow velocity higher than in the case of an isolated cylinder and covers a larger range of velocity.

(b) Despite the absence of the hysteresis loop and its discontinuities, flow visualization of the downstream cylinder near-wake showed the presence of two vortex patterns around the resonance, one below the resonance velocity which is of the Kármán type and another above the resonance velocity.

(c) As the spacing ratio L/D of the tandem arrangement is gradually increased from 7 to 25, the synchronization region covers a smaller range, and the maximum amplitude of the

Aeolian oscillations as well as the velocity for which this maximum occurs are slightly reduced.

(d) For a tandem arrangement with $L/D = 7$ and 8·5, the downstream cylinder exhibits a combination of vortex-induced vibrations and wake galloping.

(e) When the blades of the model supporting system are oriented in the direction $\alpha = 45^\circ$, the model is observed to vibrate in two different and stable planes; the first corresponding to the blades constraint ($\alpha = 45^\circ$) and the second almost perpendicular to the first. At some critical velocities, the vibration switches from one plane to the other.

(f) In the case of a staggered arrangement with a fixed $L/D = 13$, an increase of the bundle inclination angle β reduces the synchronization onset velocity and the synchronization region. The response of the downstream cylinder tends to that of an isolated one as β is increased. Beyond $\beta = 20^\circ$, the downstream cylinder is outside the wake and behaves as if it were isolated.

(g) The critical curve separating the 2S and 2P mode regions of vortex pattern (isolated cylinder) shifts towards higher velocities when the downstream cylinder is partially submerged in the wake of the upstream cylinder ($\beta = 15^\circ$). For the same reduced velocity, the bifurcation occurs at lower amplitudes for $\beta = 15^\circ$ than for 20°. Beyond $\beta = 20^\circ$ the critical curve coincides with that of an isolated cylinder.

ACKNOWLEDGEMENT

The authors gratefully acknowledge the financial support of Hydro-Québec and the Natural Science and Engineering Research Council of Canada (NSERC).

References

Bearman, P. W. 1984 Vortex shedding from oscillating bluff bodies. *Annual Review of Fluid Mechanics* **16,** 195–222.

Bishop, R. E. D. & Hassan, A. Y. 1964 The lift and drag forces on a circular cylinder in a flowing fluid. *Proceedings of the Royal Society* (*London*) A**277,** 51–75.

Blevins, R. D. 1990 *Flow-Induced Vibrations*, 2nd edition. New York: Van Nostrand Reinhold.

Bokaian, A. & Geoola, F. 1984 Wake-induced galloping of two interfering circular cylinders. *Journal of Fluid Mechanics* **146,** 383–415.

Brika, D. & Laneville, A. 1993 Vortex-induced vibrations of a long flexible circular cylinder. *Journal of Fluid Mechanics* **250,** 481–508.

Brika, D. & Laneville, A. 1995a An experimental study of the Aeolian vibrations of a flexible circular cylinder vibrating at different incident planes. *Journal of Fluids and Structures* **9,** 371–391.

Brika, D. & Laneville, A. 1995b The hysteresis and bifurcation phenomena in the Aeolian vibrations of a circular cylinder. In *Flow-Induced Vibration* (ed.) P. W. Bearman, pp. 27–38, Balkema.

Chen, S. S. 1986 A review of flow-induced vibration of two circular cylinders in crossflow. *ASME Journal of Pressure Vessel Technology* **108,** 382–393.

Cooper, K. R. & Wardlaw, R. L. 1971 Aeroelastic instabilities in wakes. *Proceedings International Conference on Wind Effects on Buildings and Structures*, pp. 647–655, Tokyo.

King, R. & Johns, D. J. 1976 Wake interaction experiments with two flexible circular cylinders in flowing water. *Journal of Sound and Vibration* **45,** 259–283.

Mahir, N. & Rockwell, D. 1996 Fortex formation from a forced system of two cylinders. Part I: Tandem arrangement. *Journal of Fluids and Structures* **10,** 473–489.

Nakayama, Y. (ed. in chief), 1988, *Visualized Flow*. Oxford: Pergamon Press.

Norberg, C. 1998 LDV-measurement in the near wake of a circular cylinder. In *1998 Conference Bluff Body Wakes and Vortex-Induced Vibration* (eds P. W. Bearman & C. H. K. Williamson), Paper No 42, Washington, D. C.

Ohya, Y., Okajima, A. & Hayashi, M. 1989 Wake interference and vortex shedding, Chap. 10. In *Encyclopedia of Fluid Mechanics* (ed. N. Cheremisinoff), Vol. **8,** pp. 322–389. Houston: Gulf Publishing Co.

Öngören, A. & Rockwell, D. 1988 Flow structure from an oscillating cylinder. Part II: Mode competition. *Journal of Fluid Mechanics* **191,** 198–xxx.

Parkinson, G. V. 1989 Phenomena and modeling of flow-induced vibrations of bluff bodies. *Progress in Aerospace Science* **26,** 169–224.

Pon, C. J., Currie, I. G. & MacDonald, R. 1989 Aeolian vibration excitation of bundle conductors. Canadian Electrical Association, Technical Report, 177 T 510.

Price, S. J. 1975 Wake-induced flutter of power transmission conductors. *Journal of Sound and Vibration* **38,** 125–147.

Ruscheweyh, H. P. 1983 Aeroelastic interference effects between slender structures. *Journal of Wind Engineering and Industrial Aerodynamics.* **14,** 129–140.

Sarpkaya, T. 1979 Vortex-induced oscillations — A selective review. *Journal of Applied Mechanics* **46,** 241–258.

Tanida, Y, Okajima, A. & Watanabe, Y. 1973 Stability of a circular cylinder oscillating in uniform flow or in a wake. *Journal of Fluid Mechanics* **61,** 769–784.

Williamson, C. H. K. & Roshko, A. 1988 Vortex formation in the wake of an oscillating cylinder. *Journal of Fluids & Structures* **2,** 355–381.

Zdero, R., Turan, O. F. & Havard, D. G. 1995 Toward understanding galloping: Near-wake study of oscillating smooth and stranded circular cylinders in forced motion. *Experimental Thermal and Fluid Science* **10,** 28–43.

Zdravkovich, M. M. 1977 Review of flow interference between two circular cylinders in various arrangements. *ASME Journal of Fluids Engineering* **99,** 618–633.

Zdravkovich, M. M. 1982 Modification of vortex shedding in the synchronization range. *ASME Journal of Fluids Engineering* **104,** 513–517.

Zdravkovich, M. M. 1988 Review of interference-induced oscillations in flow past two parallel circular cylinders in various arrangements. *Journal of Wind Engineering and Industrial Aerodynamics* **28,** 183–200.